Computer Modeling in Engineering & Sciences

Tech Science Press

https://doi.org/10.32604/cmes.2026.080484

ARTICLE

Intelligent Modeling of Thin Plate Buckling via Machine Learning

Salamat Ullah[1,2,*], Muhammad Zahid[3], Khaled Aati[4], Abdulrahman Abbadi[4], Haroon Ijaz[5] and Ali Qabur[4]

[1]Center for Mechanics Plus under Extreme Environments, Ningbo University, Ningbo, China
[2]Department of Software Engineering, Faculty of Science & Technology, ILMA University, Karachi, Pakistan
[3]School of Engineering, The University of British Columbia, Okanagan, 1137 Alumni Avenue, Kelowna, BC, Canada
[4]Department of Civil and Architectural Engineering, Jazan University, Jazan, 45142, Saudi Arabia
[5]State Key Laboratory of CAD&CG, Zhejiang University, Hangzhou, China

*Corresponding Author: Salamat Ullah. Email: salamatullah@nbu.edu.cn

Received: 10 February 2026; Accepted: 10 April 2026; Published: 27 May 2026

ABSTRACT: Designing thin-walled plate structures is challenging due to their susceptibility to various forms of structural instability. In addition, the substantial computational cost of finite element analyses, especially in optimization scenarios, underscores the need for efficient and reliable surrogate models. To address this challenge, the present study employs machine learning (ML) techniques to predict the buckling response of thin plates under complex boundary conditions. Four ML models, including XGBoost, CatBoost, Light GBM, and Random Forest, are developed to predict the buckling coefficient based on input features, including aspect ratio, boundary condition, and compressive loading pattern. The training data for these models is generated using the finite integral transform method. Model performance is rigorously evaluated, with all four algorithms demonstrating strong predictive capabilities. Among them, XGBoost demonstrates the superior predictive performance, achieving an R^2 value of 0.99. To gain deeper insights into feature influence, SHAP analysis is conducted, revealing that the aspect ratio has the greatest influence on buckling coefficient, followed by boundary conditions and compressive loading. By adopting gradient-boosting approaches, the proposed framework demonstrates improved generalization and reduced overfitting, with potential applicability to structural optimization. The results suggest that integrating machine learning with structural analysis can serve as a computationally efficient approach for the design and optimization of thin-walled plates.

KEYWORDS: Buckling behavior; rectangular thin plates; machine learning; XGboost; SHAP analysis

1 Introduction

Plates are fundamental structural elements widely employed in civil engineering works, where they play a critical role in supporting loads in buildings, bridges, offshore platforms, and other large-scale infrastructure. Plate buckling [1] is a well-known limit state in civil structures and a recurring design constraint because it can erode both safety and serviceability. The move toward high-rise buildings, longer spans, and slimmer components has raised the margin for instability and prompted focused work on materials, design rules, and analysis routines that improve resilience. In practice, engineers now need predictions of buckling that are accurate enough to support both safety checks and material economy. Because buckling depends strongly on nonlinear response and boundary conditions, analysis tools must reflect those features to be credible at modern structural scales [2].

Numerical methods now make much of this feasible and improve the study of plate buckling, addressing key challenges in structural stability. Finite differences remain a workhorse for approximate plate-buckling solutions due to their direct setup and flexibility [3,4]. Differential quadrature offers high accuracy for thin rectangular plates under varied supports and loadings [5–7]. Discrete singular convolution supplies an efficient route to difficult boundary-value problems in plates [8,9]. Meshfree formulations have also proved effective for coupled buckling–vibration studies of composite plates and laminates under compression [10,11]. Specialized schemes—the extended Kantorovich method for stepped plates and the exact finite strip method for moderately thick plates—deliver precise results by blending classical and higher-order theories [12,13]. More general frameworks, notably the finite element method [14–16] and the Ritz energy approach [17–20], are used across plate types because they balance accuracy with computational practicality. Together, these methods have sharpened both the fidelity and the reach of plate-buckling analysis.

Numerical techniques, although effective in various engineering applications, are inherently approximate, which limits their exactness and presents a primary drawback. To overcome this limitation, benchmark analytical solutions are essential, as they not only validate numerical and approximate methods but also enhance the reliability of new approaches and deepen insight into complex plate behaviors. Analytical methods, such as the Navier [21–24] and Lévy solutions [25,26], provide precise results for plate problems. For instance, investigations into the buckling of Reddy plates considering both isotropic and orthotropic materials have primarily addressed classical boundary conditions, producing closed-form solutions for buckling coefficients and mode shapes of orthotropic plates [27,28]. Furthermore, the influence of geometric factors such as aspect ratio and fiber orientation has been analyzed, with separation-of-variable techniques applied to derive closed-form solutions for vibration and thermal buckling under classical boundaries [29]. Beyond these, nonlocal elasticity theory has led to the development of an analytical approach for rectangular nanoplates [30]. Lim et al. established symplectic elasticity as an exact analytical framework for rectangular plates, demonstrating bending and free vibration solutions that provided a rigorous Hamiltonian foundation for subsequent plate analyses [31,32]. Lim and Xu later synthesized the theory and applications of symplectic elasticity, clarifying its unified formulation and highlighting its broad usefulness for static and dynamic structural mechanics problems in practice [33]. Li et al. developed new analytical free vibration solutions for orthotropic rectangular plates, showing that the symplectic approach can effectively capture anisotropic plate behavior under complex vibration conditions [34]. They also extended the method to rectangular thick plates with a free corner, demonstrating its applicability to geometrically challenging boundary configurations [35]. For rectangular thin plates resting on multiple point supports, the symplectic superposition method provided accurate analytic vibration solutions and broadened its usefulness for discrete support problems [36]. The approach is further applied to doubly curved shallow shells and thin plates on elastic foundations, confirming its versatility for both shell vibration and plate bending analyses [37,38]. They extended the symplectic superposition method to benchmark flexure solutions for rectangular thick plates and to buckling analysis of thin plates with two free adjacent edges, demonstrating the method's effectiveness for both deformation and stability problems under challenging boundary conditions [39,40]. Asemi and Shariyat, and their coworker investigated the stability behavior of advanced heterogeneous plates using rigorous three-dimensional elasticity formulations [41]. They examined the post-buckling behavior of functionally graded auxetic plates, showing that negative Poisson's ratios and elastic foundation stiffness significantly influence deformation patterns and stability characteristics. In another study, a three-dimensional Hermitian finite element formulation is used to analyze buckling of heterogeneous FGM plates under combined loading conditions, including biaxial compression, shear, and tension–compression, providing highly accurate stability predictions [42].

Both numerical and analytical methods in the mechanics of plate structures have notable shortcomings. Numerical methods, although widely used, are approximate and often require simplifications that limit their accuracy, particularly under complex boundary conditions or irregular geometries. While analytical methods are generally efficient once a closed-form solution is available, deriving these solutions for different boundary conditions and loading configurations often involves mathematically complicated formulations and lengthy derivation procedures. In addition, conducting extensive parametric studies using analytical formulations may require considerable time and effort. In contrast, numerical methods such as the finite element method require significant computational resources, particularly for large-scale problems or when repeated simulations are needed. These limitations highlight the need for advanced techniques to overcome computational cost and accuracy issues.

AI and machine ML are progressing areas of computer science, enabling the creation of systems that emulate human cognition and generate data-driven models for addressing complex problems with high accuracy. In engineering applications, well-designed ML models can reveal hidden correlations between input parameters and predicted outcomes while aligning with core physical principles. Despite the broad adoption of AI and ML across numerous industries, their integration into structural engineering remains limited, even as research continues to demonstrate their remarkable accuracy and transformative potential. Since the earliest contributions to this field [43–47], the body of research on ML in civil and structural engineering has expanded at an accelerating rate.

Recent advances in computational structural engineering have increasingly integrated intelligent algorithms with mechanics-based modeling to address complex structural problems, including machine learning–finite element hybrid frameworks for ground deformation prediction [48], neural-network-based approaches for uncertain structural response analysis [49], hybrid evolutionary algorithms for structural topology optimization [50], quantum-based strategies for structural reliability optimization [51], and advanced manufacturing-oriented analysis of thin-walled structural components [52]. Structural monitoring has also advanced through a measurement-based adaptive substructure identification framework for dynamic response reconstruction [53] and a multimodal self-sensing electronic gasket for pipeline structural health monitoring [54]. In addition, thin-walled system modeling has been improved by a tube-core sandwich-enhanced configuration for investigating dynamic behavior [55] and an analytical computational framework for predicting the dynamic plastic response of sandwich beams under ice impact [56]. Similarly, ensemble learning methods, including adaptive boosting, extreme gradient boosting, and gradient tree boosting, have accurately predicted compressive strength in conventional, high-performance, and phase-change-material-integrated cementitious composites, confirming the growing reliability of data-driven approaches in engineering practice [57–60]. Nevertheless, the use of ML in structural mechanics, particularly in investigating the mechanical behavior of plate structures, remains limited. Recently, ML algorithms such as a multi-layer Artificial Neural Network (ANN) have been employed in predicting the buckling behavior of plate structures. Moreover, it predicts elastic critical buckling loads and to performs modal decomposition of thin-walled channel members under axial compression, achieving prediction accuracies of up to 98% [61]. Similarly, a data-driven ANN model is developed to predict the critical buckling loads of functionally graded material (FGM) plates, offering a simpler alternative to complex analytical methods, with 99.95% accuracy [62]. The model showed that the critical buckling loads are insignificantly influenced by variations in the volume fraction and modulus of elasticity ratios of the materials. Additionally, seven ML models are developed to predict elastic buckling and ultimate loads, leveraging validated finite element data and achieving high accuracy [63].

ML techniques, particularly Deep Learning (DL), have been used to develop surrogate models for fiber steering composite cylinders under bending loads, outperforming models like Random Forest, Decision

Tree, and Multiple Linear Regression with more stable results and improved generalization [64]. Gene expression programming, an ML algorithm, has been developed to predict the buckling behavior of rectangular thin plates with both classical and non-classical types of boundary conditions. The input data is derived using an analytical technique, with the Gene expression programming model accurately predicting the results [65]. Additionally, gradient boosting methods such as XGBoost have been employed to predict the elastic buckling coefficient with notable precision. Interpretability analyses using SHAP identified the aspect ratio of the plate as the most influential parameter governing buckling strength [66].

Machine learning (ML) is increasingly used to build task-specific tools for structural engineering. In plate problems, well-trained models can evaluate buckling behavior quickly across varied loading and boundary conditions, including nonlinear responses and non-classical edges. Uptake is still slowed by unfamiliarity and the need for validation, but that gap is narrowing as education, datasets, and case studies accumulate. In this study, ML is used to estimate the plate buckling coefficient from data derived from analysis and experiments, linking closed-form theory with design checks used in practice and providing a route to more efficient plate sizing.

Relative to traditional workflows, ML surrogates can reduce repeated high-fidelity finite-element runs when the design variables remain within the model's training domain. This is useful early in design, when time and software expertise are limited. By contrast, simplified FE analyses—often adopted under schedule pressure—tend to trade accuracy for speed and can push safety factors and material usage higher than necessary. Analytical solutions remain valuable baselines, but they become cumbersome when parameters or boundary conditions change, since new derivations are required and the algebra grows quickly. In that setting, a vetted ML model is a practical complement—not a replacement—for detailed FE studies on the final design.

In this work, we develop predictive models for the buckling coefficient of thin plates across a range of aspect ratios, boundary conditions, and material properties. Because these configurations exhibit strong nonlinear interactions and are costly to resolve with high-fidelity finite-element (FE) analyses, we frame the problem as supervised learning and evaluate a suite of tabular learners—XGBoost, CatBoost, Random Forest, and LightGBM. Our aim is accurate prediction with models whose behavior can be examined rather than treated as opaque surrogates. To that end, we pair the trained predictors with post-hoc interpretability tools, using SHapley Additive exPlanations (SHAP) and complementary statistical diagnostics to attribute variance in the buckling coefficient to specific inputs and to quantify feature interactions (e.g., aspect ratio with edge restraint). This combination provides design-relevant accuracy while preserving transparency in how the models arrive at their estimates.

The study addresses the computational inefficiency and limited interpretability associated with conventional approaches for predicting the buckling behavior of thin plates under varying boundary conditions and loading scenarios. While existing studies have primarily relied on finite element methods or ANN-based models, they often involve high computational cost or lack transparency in model behavior. The novelty of this work lies in the development of gradient-boosting-based surrogate models trained on analytically generated data, enabling accurate and computationally efficient prediction of buckling coefficients across a wide parametric space. In addition, the integration of SHAP-based interpretability provides quantitative insight into the influence and interaction of key parameters such as aspect ratio, boundary conditions, and loading configurations. This combined framework offers a data-driven yet interpretable approach for understanding and approximating thin-plate buckling behavior.

2 Governing Equation and Finite Integral Transform Expression

A rectangular thin plate of uniform thickness h, length a, and width b is considered, with the coordinate system illustrated in Fig. 1. According to classical Kirchhoff plate theory, the buckling behavior of thin plate under a biaxial normal loads N_x and N_y, uniformly distributed along x and y directions can be formulated as:

$$\frac{\partial^4 W}{\partial x^4} + 2\frac{\partial^4 W}{\partial x^2 \partial y^2} + \frac{\partial^4 W}{\partial y^4} + \frac{N_x}{D}\frac{\partial^2 W}{\partial x^2} + \frac{N_y}{D}\frac{\partial^2 W}{\partial y^2} = 0 \tag{1}$$

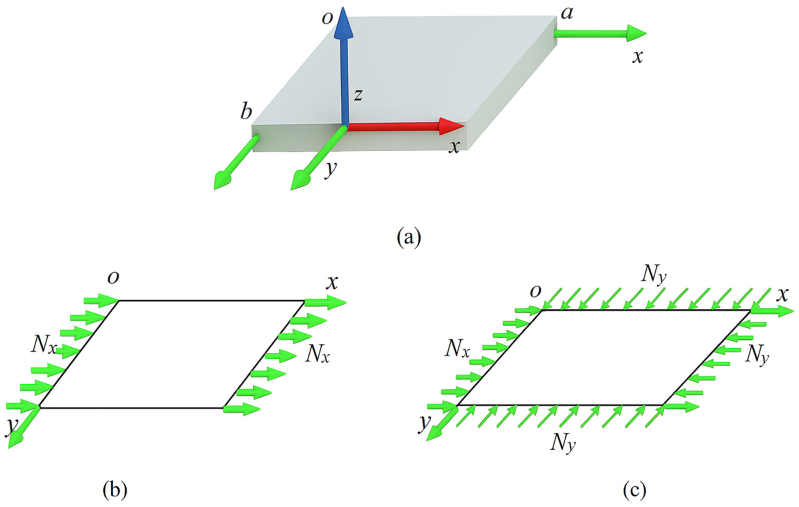

Figure 1: (**a**) Rectangular thin plate (**b**) plate under uniaxial compression (**c**) plate under biaxial compression.

Here $D = Eh^3/12\left(1-\mu^2\right)$ represents the flexural rigidity of the plate, where E denotes Young's modulus and μ is the Poisson's ratios of plate, respectively. The out-of-plane displacement $W(x, y)$ is expressed as a function of independent variables x and y defined over the rectangular domain $0 \le x \le a$ and $0 \le y \le b$.

Here double finite sine integral transform is given as:

$$W_{mn} = \int_0^a \int_0^b W(x, y) \sin(\alpha_m x) \sin(\beta_n y)\, \mathrm{d}x\mathrm{d}y \tag{2}$$

The corresponding inverse form can be written as:

$$W(x, y) = \frac{4}{ab} \sum_{m=1}^{\infty} \sum_{n=1}^{\infty} W_{mn} \sin(\alpha_m x) \sin(\beta_n y) \tag{3}$$

here $\alpha_m = m\pi/a$; $\beta_n = n\pi/b$.

The analysis explores a comprehensive range of aspect ratios, specifically 0.5, 1, 1.5, 2, 2.5, 3, 3.5, 4, 4.5, and 5, to evaluate the influence of plate geometry on buckling behavior. The investigation considers plates subjected to both uniaxial and biaxial compressive loading scenarios, providing insights into the stability characteristics under different loading conditions. To define boundary conditions, the study adopts a systematic nomenclature following an anticlockwise order starting from $x = 0$, where clamped, simply supported, and free edges are denoted as "C", "S", and "F", respectively. A diverse set of boundary conditions is examined, including configurations such as CCCC, CCCS, CCSS, CCSC, CFCF, CFSF, SFSF, CCSC, and CSSC, to account for practical and theoretical scenarios in engineering applications. This detailed approach

enables a nuanced understanding of the interplay between boundary constraints and buckling resistance, enhancing the applicability of classical plate theory to real-world structural systems.

3 Data Collection

In order to develop machine learning (ML) models, we generated data by analyzing the buckling behavior of thin plates. It should be noted that the dataset used in this study is generated from analytical solutions derived using the finite integral transform method, which are based on classical plate buckling theory. The purpose of applying machine learning in this context is not to replace the analytical formulation, but rather to develop a data-driven surrogate model that can rapidly approximate the analytical results across a wide parameter space. Although analytical solutions provide accurate predictions for idealized conditions, their application can become mathematically complex and computationally cumbersome when repeatedly evaluated for different combinations of geometric parameters, boundary conditions, and loading configurations. In contrast, once trained, machine learning models can provide instant predictions of the buckling coefficient, enabling efficient parametric studies, design optimization, and real-time evaluation in structural design frameworks. Therefore, the ML models serve as a computationally efficient approximation of the analytical solution, particularly useful in large-scale design exploration problems. This analysis considered isotropic material and examined a range of aspect ratios between 0.5 and 5. Additionally, the study incorporated seven different boundary condition configurations (CCCC, CCCS, CCSC, CCSS, CFCF, CFSF, and SFSF) to provide a comprehensive evaluation of buckling behavior. In the ML framework, the buckling coefficient is treated as the target output, while the input variables include material type, aspect ratio, and boundary conditions. For computational processing, boundary conditions are encoded numerically, assigning values from 1 to 7 corresponding to the specific configurations listed above.

To ensure the quality and reliability of the dataset, several validation checks are performed. A threshold of 20% deviation is defined to identify potential numerical artifacts or convergence issues; however, no data points exceeded this threshold, and thus no samples are removed from the dataset. Randomly, we split the refined dataset into two groups: one is used for training, and the other is for testing the model. The training dataset is used to construct the model through an evolutionary learning approach, while the test dataset serves to assess model performance on previously unseen data. Prior to model development, a thorough parameter selection process is carried out to determine which inputs most significantly influence the buckling coefficient. The selection of input variables for the machine learning models is guided by both mechanics-based considerations and preliminary statistical evaluation. Initially, several candidate parameters related to plate geometry, loading conditions, and support constraints are considered. Based on classical plate buckling theory, parameters such as the aspect ratio (a/b), boundary condition configuration, and loading pattern (uniaxial or biaxial compression) are known to significantly influence the critical buckling coefficient. Therefore, these parameters are identified as the primary variables governing the structural stability behavior. In addition to the theoretical basis, exploratory data analysis and preliminary model training are conducted to evaluate the sensitivity of the buckling coefficient to the candidate variables. Parameters that consistently showed strong influence on prediction accuracy and model stability are retained, while redundant or weak predictors are excluded to avoid unnecessary model complexity. As a result, the final feature set used for the machine learning models includes aspect ratio, boundary condition type, and loading configuration, which together capture the dominant geometric and mechanical factors controlling thin-plate buckling behavior.

4 Methodology

In the literature, a variety of machine learning algorithms have been used to predict the buckling loads of perforated steel beams, including decision trees, random forests, k-nearest neighbors, gradient boosting approaches, XGBoost, LightGBM, and models that include categorical feature processing. The machine learning algorithms employed in this study, XGBoost, CatBoost, LightGBM, and Random Forest, are selected because they represent advanced tree-based ensemble learning techniques that have demonstrated strong performance for structured engineering datasets. Plate buckling prediction involves nonlinear interactions between geometric parameters, loading conditions, and boundary constraints, which are effectively captured by decision-tree-based ensemble methods. Gradient boosting algorithms such as XGBoost, CatBoost, and LightGBM are particularly known for their high predictive accuracy, regularization mechanisms, and ability to model complex nonlinear relationships. In contrast, Random Forest, which is based on the bagging ensemble strategy, provides a reliable baseline model with strong robustness and reduced overfitting. Including both boosting-based and bagging-based methods allows a balanced comparison of different ensemble learning strategies and helps identify the most suitable model for predicting the buckling coefficient of thin plates. These algorithms have demonstrated excellent predictive performance for both elastic and ultimate buckling loads in steel cellular beams. The results from the models are closely similar to the results obtained from numerical simulations. In a significant research, Kaveh and colleagues created ML-based models to estimate the ultimate buckling stress of composite cylinders with varying stiffness distributions. Their approach demonstrated how ML can successfully account for differences in material and geometric features. Similarly, other researchers used machine learning to estimate the elastic buckling coefficients of diagonally strengthened plates under various loading circumstances, including shear, bending, and axial compression. SHapley Additive ExPlanations (SHAP) research revealed that the plate's aspect ratio is the most important factor in determining buckling resistance, followed by the interaction ratio of applied loads and the stiffener's flexural and torsional rigidity. Another example is the work of Mojtabaei et al., who used multi-layer feed-forward artificial neural networks (ANNs) to simulate the buckling behavior of thin-walled channel sections under combined axial and bending loads. Geometric variables, including cross-sectional dimensions, plate thickness, stiffener layout, and member length, are used as model inputs. With these descriptors, the models estimate the critical buckling load and indicate the governing buckling mode with high fidelity across varied test scenarios. Collectively, the findings highlight where ML offers the greatest value in structural mechanics: problems that strain classical workflows because of high computational cost or wide parametric design spaces. As the underlying algorithms mature, integration of ML into routine analysis and design should improve both the speed and the reproducibility of stability checks and optimization studies.

This section sets out the learning framework in detail. We first describe the training procedures and activation functions considered when selecting a suitable network architecture. We then specify the evaluation measures used to compare candidates and to judge robustness. In particular, we document the training strategies adopted to establish an effective architecture and list the activation functions tested. Finally, we report the metrics used to assess performance and stability so that the comparison among models is transparent and repeatable. In short, this section provides a full account of the proposed methodology and of the criteria used to evaluate it.

4.1 XGBoost

XGBoost is an open-source implementation of gradient boosting with decision trees as base learners. It has been widely adopted for both regression and classification because it scales to large datasets, handles missing entries natively, and offers competitive accuracy with efficient training. In XGBoost, a sequence of shallow trees is built to reduce the current loss; at each boosting round, a new tree is fit to the negative

gradient (the residual) of the objective with respect to the model's predictions. The ensemble prediction is the sum of the outputs from all trees, and training proceeds by minimizing a specified loss, mean squared error for regression or cross-entropy for classification, augmented by regularization to control model complexity. Overfitting and improving generalization issues are addressed through practical features, that are early stopping and built-in regularization.

The XGBoost algorithm can be formalized mathematically as shown in Eq. (4) as a series of decision trees, where each tree tries to optimize (minimize) the loss function as per the residuals from the previous trees.

$$Z = H(x_i) = \sum_{t=1}^{T} f_t(x_i) \tag{4}$$

here, independent variables are indicated by x_i, while the output function in each tree by $f_t(x_i)$. The gradient of the loss function concerning the predicted values is calculated and used to update the predicted values for the next iteration. The trees in XGBoost are typically decision trees. These trees split the feature space into smaller regions and predict a constant value within each region. The splits are chosen to minimize the loss function, and the final prediction is a weighted sum of the predictions from each tree. The weights are optimized during training to reduce the loss function. Fig. 2 illustrates the XGBoost schematic.

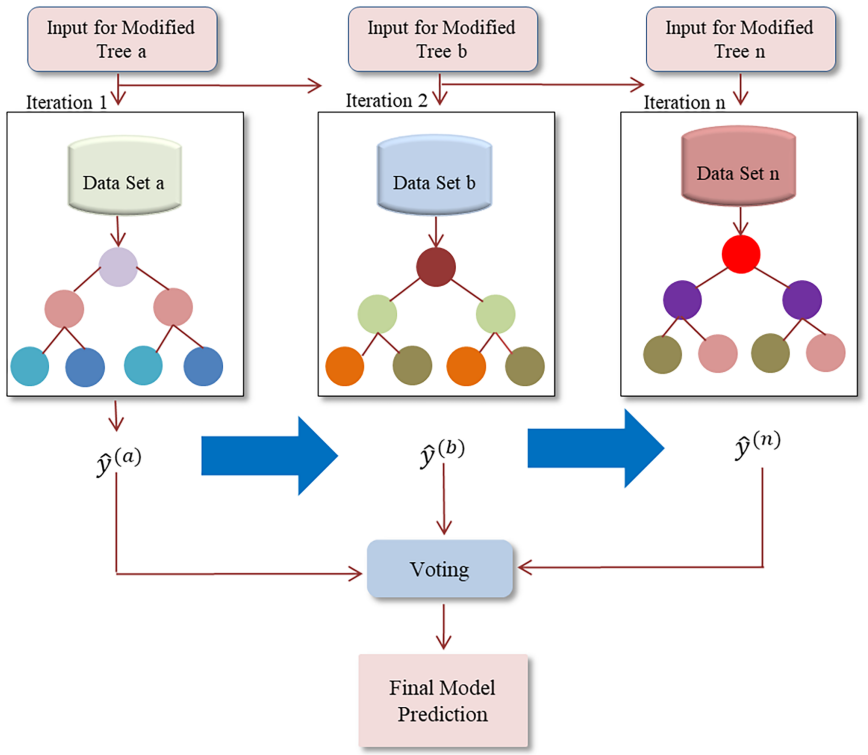

Figure 2: Illustration of XGBoost.

4.2 CatBoost

We included CatBoost in the model suite because it handles categorical encodings and missing entries without *ad-hoc* preprocessing, which keeps the pipeline aligned with the shared feature set used throughout this study (aspect ratio, boundary-condition encoding, and loading descriptors). Rather than

one-hot expanding high-cardinality categories, CatBoost computes permutation-based target statistics in an "ordered" manner to limit leakage; this proved useful for the boundary labels used here and avoided the sparsity that would have resulted from naïve encoding. Within our framework, CatBoost is trained as an additive ensemble of shallow regression trees, selected to balance bias and variance under the same train/test protocol applied to the other boosters. The following equation shows how the prediction is updated at each stage carried out:

$$Z = F(x_i) = \sum_{j=1}^{j} b_j 1_{\{x \in R_j\}} \tag{5}$$

and is updated stage-by-stage according to the generic boosting step referenced in Eq. (5). At iteration t, a new tree b_j is fitted to the negative gradient of the chosen objective with respect to the current prediction $\mathrm{F}(x_{j-1})$. Leaves take constant values over disjoint regions $\{\mathrm{Rt}, \ell\}$, and the update $\mathrm{F}(x_j)$ uses a learning rate η chosen during hyperparameter search. This construction matches the notation introduced earlier and keeps CatBoost directly comparable with XGBoost and LightGBM in the results that follow (see Eq. (5)).

For the objectives used in this paper, we employ squared-error loss for regression of the buckling coefficient; cross-entropy and multiclass objectives are available in the library, but are not required here. Regularization is applied through depth constraints and penalties on leaf weights, with early stopping based on validation loss to prevent overfitting. Two implementation details are pertinent to our dataset: (i) "ordered boosting," which computes category statistics using only prior samples in an iteration-specific permutation, reducing prediction shift when boundary categories are informative; and (ii) native routing of missing values, allowing "NaN" to follow a dedicated branch when that choice improves the objective. Training uses the same splits, feature definitions, and evaluation metrics as the other models to ensure a like-for-like comparison in Section 5.1. Fig. 2 provides a schematic of the boosting workflow used across the tree-based models, including CatBoost.

4.3 LightGBM

LightGBM is included as a complementary gradient-boosted tree framework that emphasizes training speed on tabular data through histogram-based splits and a leaf-wise (best-first) growth policy. In our setting, where feature interactions between aspect ratio and boundary conditions matter, the histogram algorithm bins continuous inputs so that split gains can be computed efficiently without scanning every unique value. In addition, Gradient-based One-Side Sampling (GOSS) and Exclusive Feature Bundling (EFB) are available to further reduce computation; we enabled histogram binning throughout and evaluated GOSS/EFB during tuning, adopting them when they improved validation error without harming stability. These choices are made to keep LightGBM's preprocessing consistent with the rest of the pipeline and to isolate algorithmic effects rather than data-engineering artifacts.

The prediction equation for a LightGBM model can be expressed mathematically as follows:

$$F_M(x) = \sum_{m=1}^{T} r_m h_m(x) \tag{6}$$

here M represents the maximum number of iterations and $h_m(x)$ denotes the base decision tree. At each round, a new tree $h_m(x)$ is fitted to the negative gradients of the loss evaluated at the current predictions. The leaf-wise growth strategy selects the single split—anywhere in the current tree—that yields the largest reduction in the objective, subject to explicit constraints on maximum depth or number of leaves to control complexity. This best-first policy can produce compact trees with strong local fits on tabular problems like

ours; to temper overfitting on smaller subsets of the boundary categories, we combine depth/leaf limits with shrinkage and early stopping, exactly as reported in Section 5.1. Figs. 3 and 4 (histogram construction and level-wise vs. leaf-wise growth) illustrate the mechanisms that differentiate LightGBM from level-wise boosters while keeping the additive prediction form unchanged.

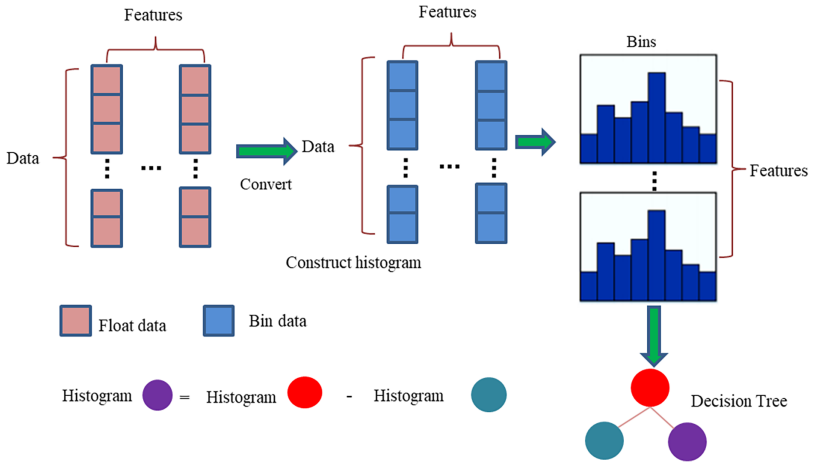

Figure 3: Histogram-based gradient boosting decision tree algorithm.

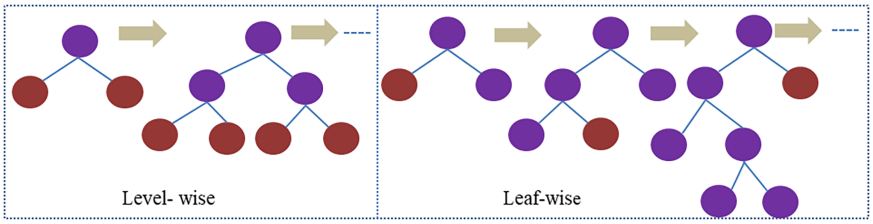

Figure 4: Expansion strategies: level-wise vs. leaf-wise.

Inference mirrors training: the final estimate of the buckling coefficient is the sum of per-tree leaf values after M rounds. Because all models in Section 4 share the same input definitions and the same evaluation criteria (R^2, RMSE, MAE, MSE), LightGBM's results can be compared directly with those from XGBoost, CatBoost, and Random Forest in Section 5, and its behavior can be interpreted within the same SHAP framework used for feature-influence analysis.

4.4 Random Forest (RF)

RF stands as a comprehensive learning method that integrates multiple decision trees to alleviate feature data correlation. RF introduces randomness by selecting samples and features, effectively mitigating the correlation among decision trees. The process involves randomly choosing an equal quantity of data from the original dataset. Subsequently, a decision tree is constructed by randomly selecting certain features. These two forms of random sampling significantly diminish the correlation between individual decision trees. This strategy aims to address potential errors arising from overfitting and, consequently, enhance the overall accuracy of the model.

The utilization of multiple trees is employed to enhance prediction performance. Let Nm represent the bootstrap sample size derived from our original data sample N to randomly grow a tree, and

X = (Xi, i = 1, 2, 3, . . ., z) represents the predictor variables. The selection of predictors is optimized at each node, ensuring the most appropriate predictor for the split is identified. The model encompasses Rt regression trees, *x* represents the test sample, and the ultimate output of the regression model is determined accordingly. Fig. 5 shows RF algorithm schematic.

$$H(x) = \frac{1}{R_t} \sum_{i=1}^{R_t} h_i(x) \tag{7}$$

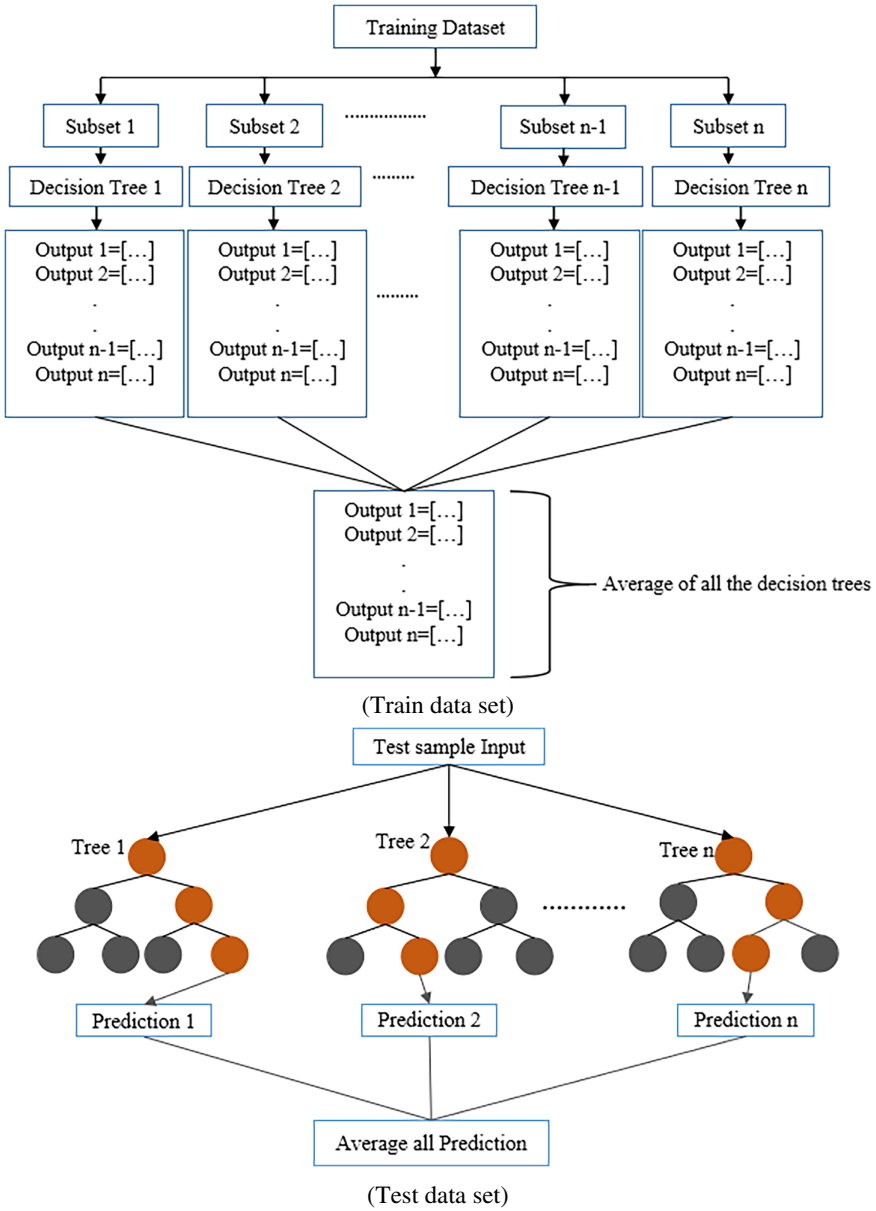

Figure 5: RF algorithm schematic.

4.5 Shapley Additive Explanations (SHAP)

One of the prominent challenges in machine learning (ML) is the lack of interpretability of its models, an aspect that has not been thoroughly addressed. To interpret the influence of input parameters on the predicted buckling coefficient, SHAP (SHapley Additive exPlanations) analysis is employed. SHAP is a game-theory-based interpretability method that quantifies the contribution of each input feature to the model prediction by computing Shapley values, which represent the marginal contribution of a feature averaged over all possible feature combinations. In this study, SHAP analysis is applied to the trained XGBoost model, which demonstrated the best predictive performance among the evaluated algorithms. The SHAP values are computed using the TreeSHAP algorithm, which is specifically optimized for tree-based ensemble models and allows efficient and consistent calculation of feature contributions. For each sample in the dataset, SHAP values are calculated for all input variables, including aspect ratio, boundary condition, and loading parameters. The overall importance of each feature is then determined by calculating the mean absolute SHAP value across the dataset, while SHAP dependence and interaction plots are used to examine nonlinear relationships and interactions between variables. Unlike traditional feature importance methods, which highlight important features without clarifying their specific impact on predictions, SHAP provides detailed insight into how each feature influences individual predictions. It captures both positive and negative contributions; features with positive SHAP values support a prediction activity prediction, while negative values suggest opposition; inactivity prediction. SHAP is based on game theory, specifically the Shapley value, and treats each feature as a "contributor" to the prediction outcome. It assigns a contribution value to each feature for a given instance, helping users understand how the model arrived at its prediction. It is employed to enhance model interpretability alongside various machine learning techniques. In this research, SHAP analysis is performed using the XGBoost algorithm.

In general, the importance of a feature i is represented by its Shapley value, as defined in Eq. (8):

$$\phi_i = \frac{1}{|N|!} \sum_{S \subseteq N\{i\}} \frac{|S|!\,(|N| - |S| - 1)!}{N} \left[f\left(SU\{i\}\right) - f\left(S\right) \right] \tag{8}$$

In this context, the value $f(S)$ represents the output of the XGBoost model, S denotes a subset of features, and N refers to the complete set of features. The Shapley value for a specific feature, say feature i (ϕi), is calculated by averaging its marginal contributions across all conceivable feature subset combinations. This strategy entails gradually adding characteristics to the subset and assessing the subsequent change in the model's prediction, which represents each feature's relevance. Because the approach is dependent on the order in which features are introduced, the presence of correlated characteristics can affect the variation in the model's output.

4.6 Accuracy Assessment of ML Models

In evaluating model fidelity, we compare test-set observations of the buckling coefficient with the corresponding predictions and quantify agreement using (R^2), RMSE, MAE, and MSE. In this study, (R^2) gauges how well the chosen inputs—aspect ratio, boundary-condition encoding, and loading pattern—account for the variance in the target response; values near 1 signal that the model captures almost all of the observed variability, while values near 0 indicate little explanatory power. MAE complements this view by reporting the typical magnitude of the residuals in the same units as the buckling coefficient, and, because it uses absolute errors, it weights small and large deviations evenly. MSE averages the squared residuals and thus emphasizes occasional large misses; its square root (RMSE) brings that penalty back to the scale of the response and is useful for comparing models when occasional outliers matter to design checks. Taken

together, these four statistics let us assess overall fit (R^2) and the practical size of the remaining error (MAE/RMSE), while MSE highlights whether any candidate achieves low variance without masking rare but consequential discrepancies. Unlike the standard deviation of residuals, which is also used to assess model correctness, MAE assigns equal weight to all mistakes, regardless of magnitude. MSE calculates the squared differences between expected and actual values and then averages those differences. It indicates the model's average squared prediction error. Another important statistical measurement is RMSE, which evaluates how far a model's predictions differ from observed values. The square root of the residuals' mean squared error is used to calculate RMSE, which is represented in the same units as the predicted variable. RMSE is similar to MAE, except it assigns greater weight to more important errors before averaging. These statistical evaluation criteria are commonly used to determine the accuracy of regression models. Each metric has advantages and disadvantages, and researchers should select the metric that is best suited to their study issue and data type.

$$R^2 = 1 - \frac{\sum_{i=1}^{n} \left(Y_{i,a} - Y_{i,e}\right)^2}{\sum_{i=1}^{n} \left(Y_{i,a} - \overline{Y}_{i,a}\right)^2}$$

$$MAE = \frac{1}{n} \sum_{i=1}^{n} \left|Y_{i,a} - Y_{i,e}\right|$$

$$MSE = \frac{1}{n} \sum_{i=1}^{n} \left(Y_{i,m} - Y_{i,e}\right)^2$$

$$RMSE = \sqrt{\frac{1}{n} \sum_{i=1}^{n} \left(Y_{i,a} - Y_{i,e}\right)^2}$$

Here $Y_{i,a}$ is the actual recommendation rate, $Y_{i,e}$ is the estimated recommendation rate, $\overline{Y}_{i,a}$ is the mean actual recommendation rate, and n refers to the total number of observations. Lower values of *MAE*, *RMSE*, and *MAPE* suggest better model performance. Conversely, a higher R^2 value, ideally approaching 1, reflects a more accurate and reliable prediction model.

5 Results and Discussion

5.1 ML Models Development and Performance

This work uses a comparative approach to assess the efficacy of multiple supervised machine learning models in predicting the buckling coefficient based on gathered data. The goal is to investigate each algorithm's predictive capabilities by training and testing on a curated dataset. To ease model construction, the dataset is separated into two subsets: 70% for training and 30% for testing. All modeling and analysis are done with Python. Each ML model is dependent on certain hyperparameters, which must be carefully tuned to reach peak performance. Proper parameter adjustment is critical for enhancing model accuracy and generalizability. In this study, hyperparameter optimization is carried out using the scikit-learn library in conjunction with a grid search technique, which systematically investigates a given range of parameter values to find the optimal configuration. Importantly, this grid-search procedure is fully reproducible, ensuring that results can be consistently verified and extended in future studies. For clarity, the explored ranges included, for example, learning rate values between 0.01–0.3, number of estimators between 100–1000, and maximum depths between 3–10. Table 1 presents the optimal hyperparameters identified for each ML model utilized in the investigation. Among these, the learning rate defines how rapidly the model adapts during training,

the number of estimators represents the total number of boosting rounds or decision trees, and max depth specifies the maximum complexity of each decision tree. By fine-tuning these essential parameters, the performance of each ML model improved dramatically. The insights gained from this optimization method not only improve prediction accuracy for this specific challenge but also provide useful guidelines for future research aimed at developing robust machine learning models for predicting plate buckling behavior.

Table 1: Tuning parameters.

Regression Method	Leaning Rate	n Estimators	Max Depth
XGBoost	0.05	600	8
CatBoost	0.01	600	10
LightGBM	0.2	400	10
RF	0.1	150	8

ML developed in this study, including Random Forest (RF), CatBoost, LightGBM, and XGBoost, are trained and evaluated using various combinations of input features, including aspect ratio, boundary conditions, and compressive loading types. These regression models are evaluated using conventional metrics, including R^2, RMSE, MAE, and MSE. Table 2 shows a comparison of the outcomes for each model on the training and testing datasets, emphasizing their prediction accuracy and generalization capabilities. XGBoost demonstrates the strongest overall performance, achieving an R^2 of 0.99 on training and 0.96 on testing, indicating excellent model fit and generalization. It also has the lowest error values across both sets, with RMSE of 0.35 (train) and 0.83 (test), and MAE of 0.19 and 0.56, respectively, reflecting highly accurate predictions. LightGBM also performs well, with an R^2 of 0.97 (train) and 0.88 (test), but its error values, particularly on the test set (RMSE = 1.35, MAE = 0.88, MSE = 1.82), suggest a slight decline in generalization compared to XGBoost. RF shows moderate performance with R^2 of 0.94 (train) and 0.90 (test), but with higher error values than XGBoost, indicating slightly less accuracy. CatBoost appears to be the weakest among the four, with lower R^2 scores (0.78 train, 0.80 test) and the highest error metrics, particularly during training (RMSE = 2.44, MSE = 5.97), suggesting that the model struggles to fit the training data and doesn't generalize as well as the others. Overall, the data indicates that XGBoost not only fits the training data very well but also maintains robust performance on unseen test data, making it the most effective model in this comparison.

Table 2: Accuracy metrics of ML methods for train and test set.

	Training (70%)				Testing (30%)			
	R^2	RMSE	MAE	MSE	R^2	RMSE	MAE	MSE
XGBoost	0.99	0.35	0.19	0.12	0.96	0.83	0.56	0.68
LightGBM	0.97	0.94	0.57	0.89	0.88	1.35	0.88	1.82
RF	0.94	1.28	0.88	1.62	0.90	1.21	0.96	1.46
CatBoost	0.78	2.44	1.34	5.97	0.80	1.75	1.24	3.06

5.2 Models Evaluation

In Fig. 6b, the XGBoost results align closely with the 45° parity line, with the red symbols clustering tightly over the full range of the buckling coefficient. The comparison between the predicted and analytical

buckling coefficients provides important insight into the predictive capability of the proposed machine learning models. As illustrated in Fig. 6, the predicted values obtained from the different algorithms generally follow the 45° parity line, indicating good agreement with the analytical solutions. Among the models considered, XGBoost exhibits the closest alignment with the analytical results, as indicated by the tight clustering of data points around the parity line and the relatively small prediction dispersion across the entire range of buckling coefficients. This behavior suggests that the gradient boosting mechanism of XGBoost effectively captures the nonlinear relationship between the geometric parameters, boundary conditions, loading configurations, and the resulting buckling coefficient. The residual spread is small and uniform, which is consistent with strong generalization on the hold-out set and limited bias at both low and high targets. Relative to CatBoost, the improvement is evident in the narrower vertical scatter and the absence of systematic drift from the line of equality. Fig. 6c reports LightGBM. The fit is sound, but the point cloud shows a wider envelope than XGBoost—most noticeably at the upper end of the response—indicating that some interactions are not captured as cleanly. The deviations are moderate rather than catastrophic; LightGBM remains usable for this dataset, but its predictions are less steady than those from XGBoost. Fig. 6d summarizes Random Forest. Accuracy sits between CatBoost and XGBoost: dispersion is smaller than CatBoost yet larger than XGBoost, and a hint of curvature suggests local bias that could be reduced with additional tuning or feature engineering. In short, Random Forest offers acceptable generalization but still leaves room for improvement in predictive fidelity.

Across models, the ranking is clear. XGBoost delivers the most reliable predictions, combining a high correlation between predictions and observations with low residual variance; the coefficients of determination reach R^2 = 0.99 on training and R^2 = 0.96 on testing, which indicates a strong fit without obvious overfitting on unseen data. LightGBM and Random Forest perform respectably but with larger test-set dispersion, while CatBoost lags in this application, showing higher residuals and more frequent departures from the parity line. These contrasts underscore why XGBoost is our preferred surrogate for predicting the buckling coefficient and why model choice matters for design-level decisions in structural engineering.

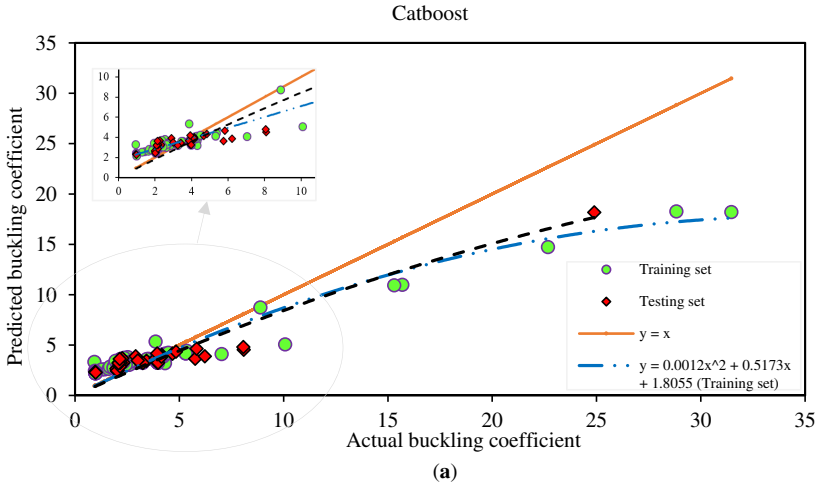

(a)

Figure 6: (Continued)

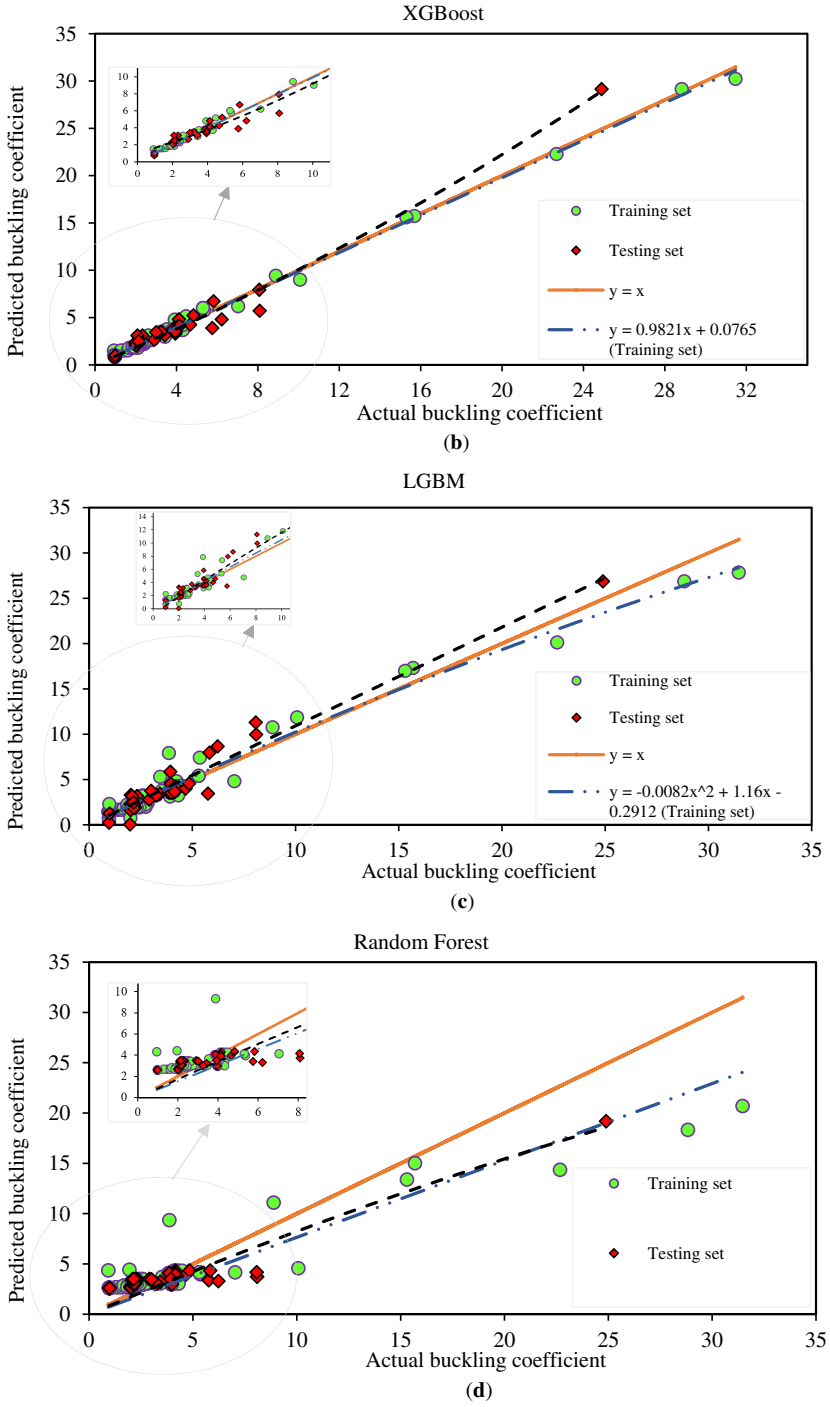

Figure 6: Comparison between predicted and actual buckling coefficients (**a**) Catboost (**b**) XGBoost (**c**) LGBM (**d**) Random Forest.

5.3 Error Analysis

The examination of four ML models (XGBoost, Random Forest, LGBM, and CatBoost) in predicting the buckling coefficient reveals significant disparities in performance, notably in terms of residual error. In contrast, Random Forest and LightGBM also demonstrate reasonable predictive capability, but their predictions exhibit slightly larger scatter around the parity line, indicating somewhat lower predictive precision compared with XGBoost. The results from CatBoost show a comparatively larger dispersion, which is consistent with the higher error metrics reported in Table 2. These differences can be attributed to variations in the learning strategies of the algorithms, particularly in how they construct decision trees and handle feature interactions. The error analysis presented in Fig. 7 further supports these observations. The residual distributions indicate that the XGBoost model produces the smallest prediction errors, while the other models exhibit progressively larger deviations from the analytical values. Overall, the results confirm that machine learning models can effectively approximate the analytical buckling solutions, with XGBoost providing the most accurate and stable predictions among the algorithms considered.

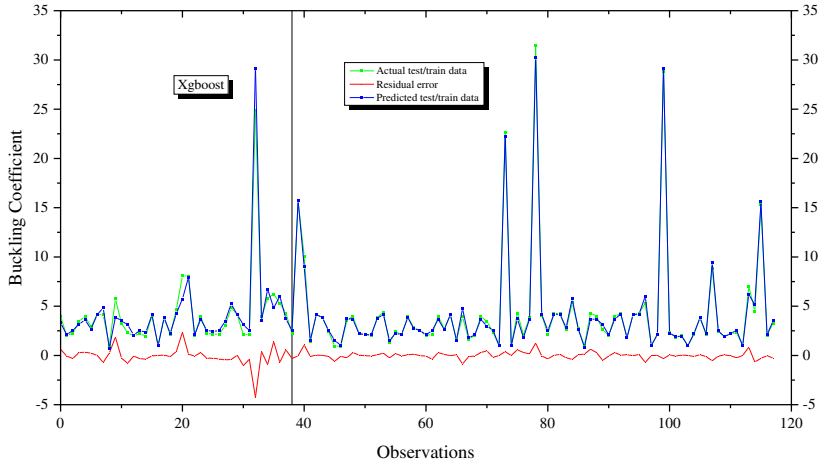

Figure 7: (Continued)

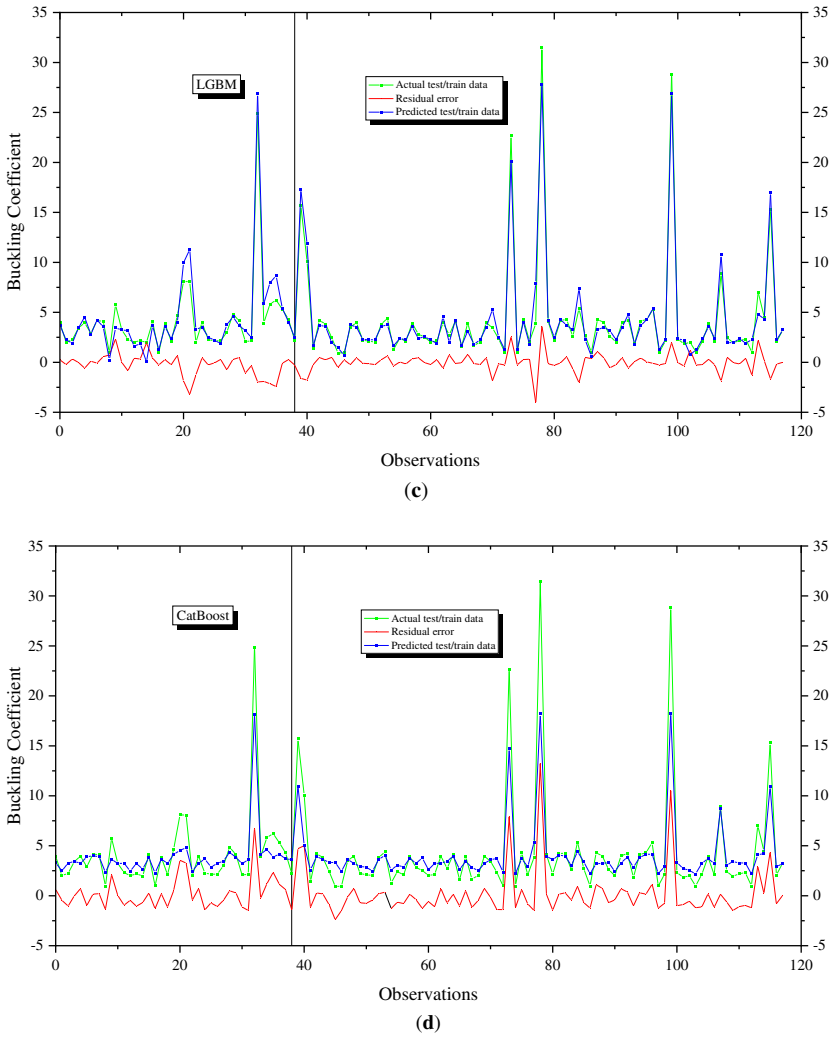

Figure 7: The absolute difference between predicted and analytical results for different models (**a**) XGboost (**b**) Random Forest (**c**) LGBM (**d**) Catboost.

In Fig. 7a, XGBoost has the smallest residual error, as seen by the narrowest red bands in the figure, implying that it provides the most accurate predictions with the least divergence from the actual data. The projected values (blue) are closely aligned with the actual values (green), indicating that XGBoost correctly identified the underlying pattern in the dataset. Random Forest, on the other hand, has a little bigger residual error, as illustrated in Fig. 7b, with red bars that are wider than those in XGBoost, indicating that its predictions stray further from the actual values. While still producing reliable results, this model does not outperform XGBoost, possibly due to its decision tree-based structure, which may not adequately represent the intricacies of the dataset. In Fig. 7c, LGBM has a considerably greater residual error and significantly wider red bands, indicating that it struggles to reliably estimate the buckling coefficient.

Despite being a powerful model, LGBM does not appear to generalize well to this particular task, potentially due to overfitting or a failure to effectively capture crucial correlations in the data. Finally, CatBoost has the highest residual error, as shown in Fig. 7d, with the widest red bars, indicating that it has the greatest trouble making accurate predictions. This could be because the dataset's complexity has an impact on the model's performance, or there is a need for more optimization, such as hyperparameter adjustment.

Overall, the models are evaluated in order of performance from least to greatest residual error: XGBoost (best), Random Forest, LGBM, and CatBoost (poorest). These findings highlight that XGBoost is the most reliable model for predicting the buckling coefficient of thin plates. A more detailed examination of the residuals is conducted to identify specific parameter combinations associated with the largest prediction errors. The analysis indicates that the highest deviations occur for extreme aspect ratios and boundary conditions involving partially constrained or free edges, such as CFSF and SFSF. These configurations tend to exhibit more complex deformation patterns and increased sensitivity to geometric variations compared with fully constrained cases (e.g., CCCC), which are more stable and easier to approximate. Despite these localized deviations, the magnitude of the errors remains relatively small, confirming that the model maintains robust predictive performance across the investigated parameter space.

The previous section found that the XGBoost model outperformed in predicting the buckling coefficient than other ML models. Despite this, many ML models are often criticized for their limited interpretability, particularly when it comes to understanding the influence of individual input variables on the final prediction. Furthermore, it is essential to interpret the model results and turn them into actionable items. To address this, the current study performed a feature importance analysis using XGBoost to rank the significance of the input parameters. XGBoost outperformed the other models primarily due to its ability to combine gradient boosting with efficient regularization, which minimizes overfitting while maintaining high accuracy. Unlike Random Forest, which builds independent trees, XGBoost builds sequential trees that correct previous errors, leading to better learning of complex nonlinear relationships. Its parallel processing capabilities and handling of missing data further improve efficiency and robustness, making it more reliable for structural prediction tasks such as plate buckling. Additionally, SHAP-based partial dependence plots are used to enhance the interpretability of the model. Through these analyses, the study aims to understand better the factors that contribute most significantly to buckling coefficient and ultimately create actionable items based on the model's findings.

5.4 Shapley Additive Explanations (SHAP)

Fig. 8 shows the SHAP summary plot, which illustrates the relative importance of different input parameters in predicting the buckling coefficient of a structural model, for a thin plate. The x-axis represents the mean of the absolute SHAP values, indicating the average contribution of each feature to the model's output prediction in terms of magnitude. Among the input variables, the Aspect Ratio (a/b) emerges as the most influential parameter, having the highest SHAP value (exceeding 2.0), which signifies its dominant role in determining the buckling behavior. This is consistent with classical buckling theory, where the aspect ratio significantly affects the critical buckling load and mode shapes. By directly aligning the SHAP results with established theoretical principles, the analysis gains credibility and interpretability. For example, classical plate theory predicts that slender plates (high aspect ratios) buckle at lower loads and exhibit distinct mode shapes, which is precisely reflected in the model's SHAP rankings. Similarly, the strong influence of boundary conditions echoes analytical solutions, where clamped edges raise stiffness and delay buckling compared to simply supported or free edges. The stress influence, with Ny exceeding Nx, also complements the theory, since buckling sensitivity depends on the alignment of loads with weaker geometric directions. Thus, SHAP not only quantifies feature effects but also reinforces classical mechanics, offering both data-driven and theory-supported insight. The Boundary Condition is the second most impactful feature, underscoring the importance of how the edges of the plate or panel are constrained; different boundary types (simply supported, clamped, or free) drastically change the stiffness distribution and thus the buckling response. The in-plane stress component Ny also has a considerable influence, more so than Nx, indicating that loading in the y-direction contributes more to variations in the buckling coefficient than loading in the x-direction,

possibly due to the geometry or loading configuration considered in the model. Overall, this SHAP analysis reveals that geometric and boundary constraints dominate the buckling response, while in-plane stress components have a secondary yet non-negligible influence. Such insights are valuable for design optimization and prioritizing parameters in structural analysis.

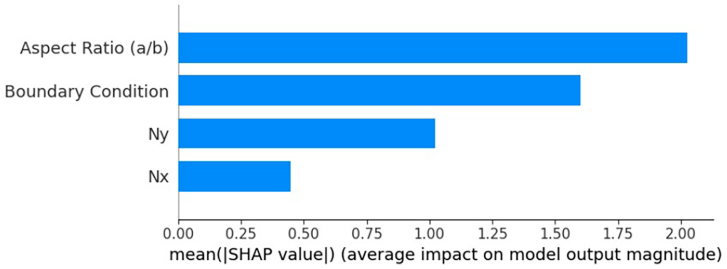

Figure 8: Influence of input variables on the buckling coefficient.

The SHAP summary plot in Fig. 8 illustrates both the magnitude and direction of each feature's influence on the predicted buckling coefficient, providing detailed insights into feature importance and behavior. The x-axis represents the SHAP value, which quantifies the impact of each feature's value on the model's output. Positive SHAP values push the prediction higher, toward an increased buckling coefficient, while negative SHAP values reduce the prediction. Each point on a line corresponds to a single instance in the dataset, colored according to the actual value of the feature for that instance: red indicates high feature values, and blue represents low feature values.

From Fig. 9, the Aspect Ratio (a/b) shows a strong influence on the buckling coefficient with both positive and negative SHAP values. Low aspect ratios (blue) tend to lower the predicted buckling coefficient (left side of the SHAP axis), while higher aspect ratios (red) push the coefficient upward, which aligns with the understanding that plates with larger a/b ratios (more slender geometries) are more prone to higher buckling capacities under certain loading conditions. The Boundary Condition also demonstrates a notable bidirectional impact. Points in the center with purplish colors suggest that intermediate values (likely different boundary condition types) can both increase or decrease the output depending on their specific configuration, indicating complex interactions. The stress component Ny (normal stress in the y-direction) shows that higher Ny values (red) are generally associated with a decrease in the buckling coefficient, while lower Ny values (blue) slightly increase it, suggesting that compressive loading in the y-direction is destabilizing. Similarly, Nx exhibits a smaller but discernible pattern: higher Nx values (red) reduce the buckling coefficient, while lower values have a minor increasing effect. Overall, the plot confirms that the buckling coefficient is highly sensitive to geometric ratios and boundary constraints, and moderately influenced by in-plane loading conditions, with both linear and nonlinear effects depending on the magnitude and direction of each feature. This plot is instrumental in understanding not just which features matter, but how they matter in practical design contexts.

The SHAP dependence plots presented in Fig. 10a–d provide a detailed understanding of how various input parameters affect the predicted buckling coefficient, along with their complex interactions. In Fig. 10a, the Aspect Ratio (a/b) shows a clear positive correlation with SHAP values, indicating that higher aspect ratios contribute to an increased buckling coefficient. The color gradient in this plot represents the boundary condition, revealing that certain support types amplify or diminish this effect for instance, clamped edges may enhance the influence of aspect ratio more than simply supported ones. Fig. 10b focuses on the boundary condition itself, showing a wide distribution of SHAP values across its range, with the color encoding the aspect ratio. This illustrates that the effect of a given boundary condition on buckling performance is

moderated by the geometry of the structure, where certain boundary types are more beneficial at specific aspect ratios. In Fig. 10c, the parameter Ny generally exhibits a negative SHAP trend, indicating that increased compressive loading reduces buckling resistance. Here, the color scale represents the Nx component, which reveals an interaction where high Nx values further intensify the destabilizing effect of Ny. In Fig. 10d, the Nx parameter itself shows a mild negative influence on buckling capacity, with the color representing boundary conditions, suggesting that the adverse effects of compressive loading along x can vary depending on edge constraints. Together, these plots not only rank feature importance but also expose nonlinear dependencies and complex interrelationships, offering valuable insights for optimizing structural designs under varied loading and boundary conditions.

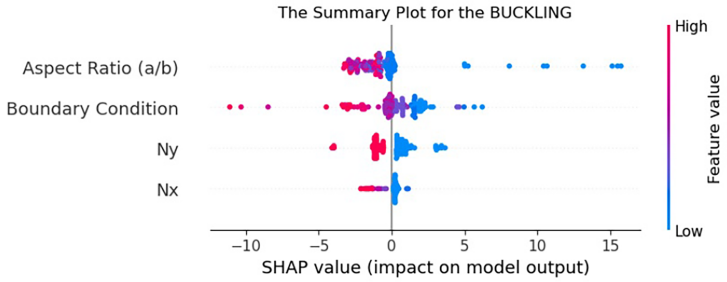

Figure 9: SHAP summary plot showing feature influence on buckling predictions; aspect ratio dominates, followed by boundary condition, Ny, and Nx, with color indicating feature value magnitude.

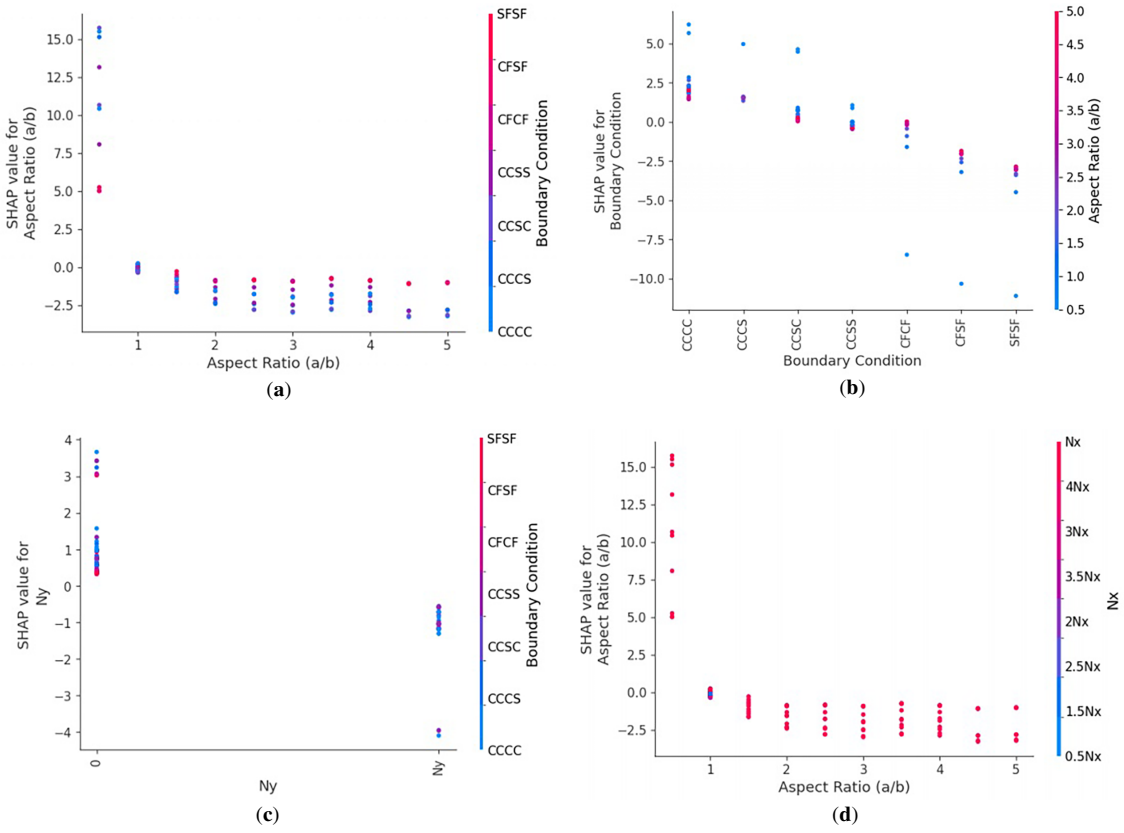

Figure 10: SHAP dependence plots.

5.5 SHAPASH Interaction Affects Plots

Fig. 11 examines how geometry and support constraints act together to shape the predicted buckling coefficient. The aspect ratio a/b remains the dominant driver: as a/b increases, thin plates become progressively more vulnerable to instability, a trend most visible for long, slender panels in Fig. 11a,b. The interaction coloring makes clear that this is not a single-factor effect. When a/b grows, the effective bending stiffness about the short direction diminishes, and the model assigns increasingly negative SHAP contributions in regions of the feature space where the plate is slender; the same geometry paired with different supports can partly offset—or amplify—this loss. In other words, the SHAPash panels show that the penalty associated with larger a/b is modulated by the companion features considered by the surrogate. Panels Fig. 11c,d turn to boundary conditions, read here in the same coding used throughout the study (C, S, F in anticlockwise order from $x = 0$). Edge restraint strongly conditions the outcome: clamped edges—which restrict both translation and rotation—consistently raise the buckling coefficient relative to simply supported or free edges, as indicated by higher SHAP contributions under C-rich encodings. The plots also show that this improvement is not uniform. For intermediate a/b, the gain from clamping is largest; at very low or very high a/b the benefit tapers as geometry, not support, limits performance. Conversely, free or partially free edges permit larger rotations near the boundary, and the model attributes more negative contributions to those cases, reflecting the easier onset of buckling. Together, these interactions reproduce familiar mechanics—stiffer edge conditions delay instability—while quantifying how much that delay depends on plate proportions.

Finally, the four panels taken as a set reinforce the need to read features jointly rather than in isolation. A high a/b plate with clamped edges does not behave like a high-a/b plate with one or more free edges; the SHAPash maps trace these nonlinear cross-effects and show where support conditions can compensate for slenderness and where they cannot. This is particularly relevant for design choices that juggle geometry, support details, and load routing: selecting a boundary configuration that lifts the SHAP contribution into the positive range for the expected a/b can reclaim safety margins without changing the planform. The interaction views in Fig. 11 therefore provide actionable guidance: they identify the a/b–boundary-condition combinations that stabilize the plate and those that drive it toward earlier buckling, informing which levers (geometry or restraint) are most effective for a given application.

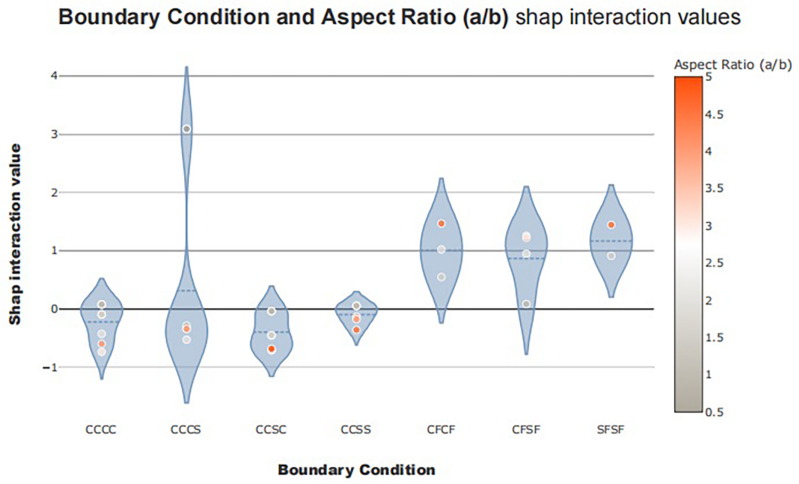

(**a**)

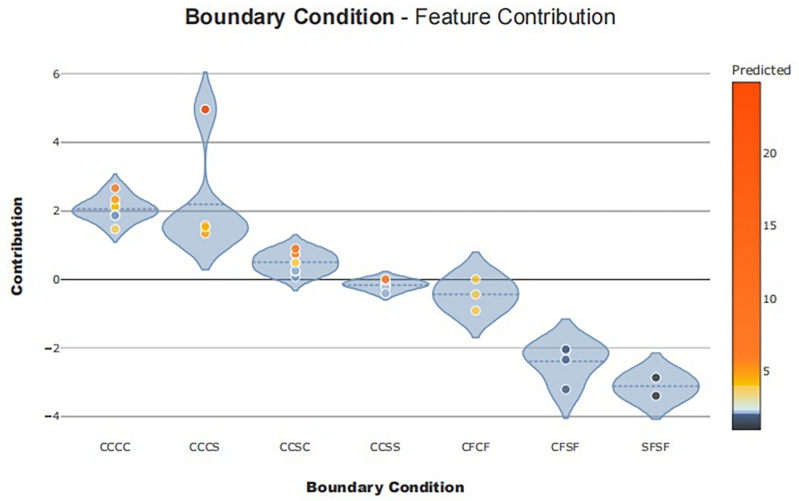

(**b**)

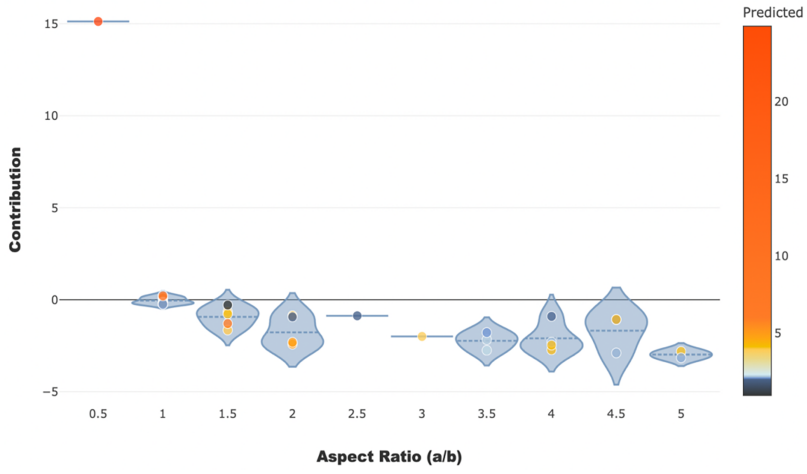

(**c**)

Figure 11: (Continued)

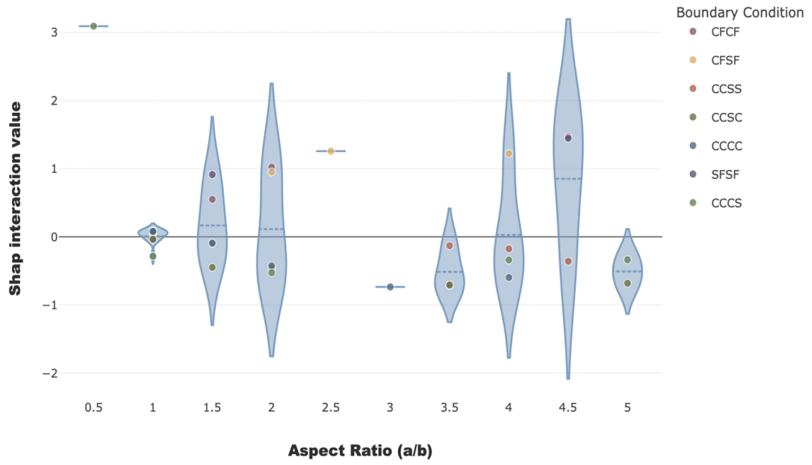

(**d**)

Figure 11: Different boundary conditions and aspect ratios have SHAPASH interaction value.

6 Conclusion

This study predicts the buckling behavior of thin-walled plates using different ML algorithms. The behavior and algorithms' performance are checked under varying boundary conditions, material properties, and aspect ratios. As a result, several models are established, including XGBoost, CatBoost, LightGBM, and Random Forest. XGBoost outperforms all other models while achieving an impressive R^2 value of 0.99 and 0.96 on the training set and on the testing set, respectively. This model showed the best fit and minimal error, validating its suitability for predicting the buckling coefficient with a high degree of reliability. The analysis further revealed, through SHAP interpretation, that the significance of the aspect ratio, boundary conditions, and compressive loading are the key factors influencing the buckling behavior of thin plates, as revealed by SHAP analysis. The finding indicated that the aspect ratio significantly impacts buckling resistance, followed by boundary conditions and compressive loading. These findings are consistent with classical buckling theory, emphasizing the significance of these parameters in designing stable thin-walled plate structures. The paper further investigated that ML offers a promising alternative to traditional methods, providing a computationally efficient, accurate, and flexible approach for predicting structural behavior, particularly with complex and nonlinear loading conditions. In addition, these approaches could be extended toward experimental validation to confirm practical applicability, or even combined with analytical models to form hybrid ML-analytical frameworks for improved accuracy. A limitation of this study is that it considers only a limited range of boundary conditions, aspect ratios, and loading cases for thin plates; therefore, further studies in this field are required to extend and validate the proposed models under broader conditions. The use of ML models importantly reduces computational costs compared to finite element methods, making them valuable tools for design optimization and real-time evaluation of structural integrity. Future work may investigate further optimization of these models and their integration into real-world engineering applications, thereby enhancing both the efficiency and reliability of structural design.

Acknowledgement: Not applicable.

Funding Statement: The authors are grateful for funding from the Deanship of Graduate Studies and Scientific Research, Jazan University, Saudi Arabia, through Project Number: JU-202503221-DGSSR-RP-2025.

Author Contributions: Conceptualization, Salamat Ullah, Muhammad Zahid and Ali Qabur; methodology, Salamat Ullah, Muhammad Zahid and Abdulrahman Abbadi; software, Haroon Ijaz, Muhammad Zahid and Khaled Aati;

validation, Salamat Ullah, Ali Qabur and Khaled Aati; formal analysis, Haroon Ijaz, Muhammad Zahid and Khaled Aati; investigation, Haroon Ijaz and Salamat Ullah; resources, Ali Qabur; data curation, Abdulrahman Abbadi; writing—original draft preparation, Salamat Ullah and Ali Qabur; writing—review and editing, Muhammad Zahid, Abdulrahman Abbadi and Khaled Aati; visualization, Salamat Ullah; supervision, Salamat Ullah; project administration, Ali Qabur; funding acquisition, Ali Qabur, Abdulrahman Abbadi and Khaled Aati. All authors reviewed and approved the final version of the manuscript.

Availability of Data and Materials: All data relevant to this study are provided in the article.

Ethics Approval: Not applicable.

Conflicts of Interest: The authors declare no conflicts of interest.

References

1. Yang Y, Xu D, Chu J, Li R. Analytic solution for buckling problem of rectangular thin plates supported by four corners with four edges free based on the symplectic superposition method. Mathematics. 2024;12(2):249. doi:10.3390/math12020249.
2. Naraidoo E, Rossi B. Local buckling load of a perforated plate—a computational study. Thin Walled Struct. 2025;215(2013):113445. doi:10.1016/j.tws.2025.113445.
3. Karamooz Ravari MR, Talebi S, Shahidi AR. Analysis of the buckling of rectangular nanoplates by use of finite-difference method. Meccanica. 2014;49(6):1443–55. doi:10.1007/s11012-014-9917-x.
4. Karamooz Ravari MR, Shahidi AR. Axisymmetric buckling of the circular annular nanoplates using finite difference method. Meccanica. 2013;48(1):135–44. doi:10.1007/s11012-012-9589-3.
5. Wang X, Huang J. Elastoplastic buckling analyses of rectangular plates under biaxial loadings by the differential qudrature method. Thin Walled Struct. 2009;47(1):14–20. doi:10.1016/j.tws.2008.04.006.
6. Jiang L, Wang Y, Wang X. Buckling analysis of stiffened circular cylindrical panels using differential quadrature element method. Thin Walled Struct. 2008;46(4):390–8. doi:10.1016/j.tws.2007.09.004.
7. Wang X, Tan M, Zhou Y. Buckling analyses of anisotropic plates and isotropic skew plates by the new version differential quadrature method. Thin Walled Struct. 2003;41(1):15–29. doi:10.1016/S0263-8231(02)00100-3.
8. Civalek O, Yavas A. Discrete singular convolution for buckling analyses of plates and columns. Struct Eng Mech. 2008;29(3):279–88. doi:10.12989/sem.2008.29.3.279.
9. Civalek Ö, Korkmaz A, Demir Ç. Discrete singular convolution approach for buckling analysis of rectangular Kirchhoff plates subjected to compressive loads on two-opposite edges. Adv Eng Softw. 2010;41(4):557–60. doi:10.1016/j.advengsoft.2009.11.002.
10. Bui TQ. Buckling analysis of simply supported composite laminates subjected to an in-plane compression load by a novel mesh-free method. Vietnam J Mech. 2011;65–78. doi:10.15625/0866-7136/33/2/39.
11. Bui TQ, Nguyen MN. A novel meshfree model for buckling and vibration analysis of rectangular orthotropic plates. Struct Eng Mech. 2011;39(4):579–98. doi:10.12989/sem.2011.39.4.579.
12. Ghannadpour SAM, Ovesy HR. The application of an exact finite strip to the buckling of symmetrically laminated composite rectangular plates and prismatic plate structures. Compos Struct. 2009;89(1):151–8. doi:10.1016/j.compstruct.2008.07.014.
13. Ovesy HR, Ghannadpour SAM, Zia-Dehkordi E. Buckling analysis of moderately thick composite plates and plate structures using an exact finite strip. Compos Struct. 2013;95:697–704. doi:10.1016/j.compstruct.2012.08.009.
14. Jeyaraj P. Buckling and free vibration behavior of an isotropic plate under nonuniform thermal load. Int J Struct Stab Dyn. 2013;13(3):1250071. doi:10.1142/s021945541250071x.
15. Aydin Komur M, Sonmez M. Elastic buckling behavior of rectangular plates with holes subjected to partial edge loading. J Constr Steel Res. 2015;112(3):54–60. doi:10.1016/j.jcsr.2015.04.020.
16. Ádány S, Visy D, Nagy R. Constrained shell finite element method, part 2: application to linear buckling analysis of thin-walled members. Thin Walled Struct. 2018;128(5):56–70. doi:10.1016/j.tws.2017.01.022.

17. Huang CS, Lee HT, Li PY, Hu KC, Lan CW, Chang MJ. Three-dimensional buckling analyses of cracked functionally graded material plates via the MLS-Ritz method. Thin Walled Struct. 2019;134(6):189–202. doi:10.1016/j.tws.2018.10.005.
18. Mijušković O, Ćorić B, Šćepanović B. Accurate buckling loads of plates with different boundary conditions under arbitrary edge compression. Int J Mech Sci. 2015;101(8):309–23. doi:10.1016/j.ijmecsci.2015.07.017.
19. Lau SCW, Hancock GJ. Buckling of thin flat-walled structures by a spline finite strip method. Thin Walled Struct. 1986;4(4):269–94. doi:10.1016/0263-8231(86)90034-0.
20. Mahendran M, Murray NW. Elastic buckling analysis of ideal thin-walled structures under combined loading using a finite strip method. Thin Walled Struct. 1986;4(5):329–62. doi:10.1016/0263-8231(86)90029-7.
21. Joshi PV, Gupta A, Jain NK, Salhotra R, Rawani AM, Ramtekkar GD. Effect of thermal environment on free vibration and buckling of partially cracked isotropic and FGM micro plates based on a non classical Kirchhoff's plate theory: an analytical approach. Int J Mech Sci. 2017;131(2):155–70. doi:10.1016/j.ijmecsci.2017.06.044.
22. Thinh TI, Tu TM, Van Long N. Free vibration of a horizontal functionally graded rectangular plate submerged in fluid medium. Ocean Eng. 2020;216(2):107593. doi:10.1016/j.oceaneng.2020.107593.
23. Akgöz B, Civalek Ö. A microstructure-dependent sinusoidal plate model based on the strain gradient elasticity theory. Acta Mech. 2015;226(7):2277–94. doi:10.1007/s00707-015-1308-4.
24. Jalaei MH, Civalek Ö. A nonlocal strain gradient refined plate theory for dynamic instability of embedded graphene sheet including thermal effects. Compos Struct. 2019;220(11):209–20. doi:10.1016/j.compstruct.2019.03.086.
25. Thai HT, Kim SE. Levy-type solution for buckling analysis of orthotropic plates based on two variable refined plate theory. Compos Struct. 2011;93(7):1738–46. doi:10.1016/j.compstruct.2011.01.012.
26. Ruocco E, Mallardo V, Minutolo V, Di Giacinto D. Analytical solution for buckling of Mindlin plates subjected to arbitrary boundary conditions. Appl Math Model. 2017;50(1):497–508. doi:10.1016/j.apm.2017.05.052.
27. Ruocco E, Reddy JN. A closed-form solution for buckling analysis of orthotropic Reddy plates and prismatic plate structures. Compos Part B Eng. 2019;169(2):258–73. doi:10.1016/j.compositesb.2019.03.015.
28. Jing Z, Sun Q, Liang K, Chen J. Closed-form critical buckling load of simply supported orthotropic plates and verification. Int J Str Stab Dyn. 2019;19(12):1950157. doi:10.1142/s0219455419501578.
29. Zhou K, Su J, Hua H. Closed form solutions for vibration and sound radiation of orthotropic plates under thermal environment. Int J Str Stab Dyn. 2018;18(7):1850098. doi:10.1142/s0219455418500980.
30. Rong D, Fan J, Lim CW, Xu X, Zhou Z. A new analytical approach for free vibration, buckling and forced vibration of rectangular nanoplates based on nonlocal elasticity theory. Int J Struct Stab Dyn. 2018;18(4):1850055. doi:10.1142/s0219455418500554.
31. Lim CW, Cui S, Yao WA. On new symplectic elasticity approach for exact bending solutions of rectangular thin plates with two opposite sides simply supported. Int J Solids Struct. 2007;44(16):5396–411. doi:10.1016/j.ijsolstr.2007.01.007.
32. Lim CW. Symplectic elasticity approach for free vibration of rectangular plates. Adv Vib Eng. 2010;9(2):159–63. doi:10.1016/j.ijengsci.2008.08.003.
33. Lim CW, Xu XS. Symplectic elasticity: theory and applications. Appl Mech Rev. 2010;63(5):050802. doi:10.1115/1.4003700.
34. Li R, Zheng X, Wang P, Wang B, Wu H, Cao Y, et al. New analytic free vibration solutions of orthotropic rectangular plates by a novel symplectic approach. Acta Mech. 2019;230(9):3087–101. doi:10.1007/s00707-019-02448-1.
35. Li R, Wang P, Wang B, Zhao C, Su Y. New analytic free vibration solutions of rectangular thick plates with a free corner by the symplectic superposition method. J Vib Acoust. 2018;140(3):031016. doi:10.1115/1.4038951.
36. Li R, Tian Y, Wang P, Shi Y, Wang B. New analytic free vibration solutions of rectangular thin plates resting on multiple point supports. Int J Mech Sci. 2016;110:53–61. doi:10.1016/j.ijmecsci.2016.03.002.
37. Li R, Zhou C, Zheng X. On new analytic free vibration solutions of doubly curved shallow shells by the symplectic superposition method within the Hamiltonian-system framework. J Vib Acoust. 2021;143(1):011002. doi:10.1115/1.4047701.
38. Li R, Zhong Y, Li M. Analytic bending solutions of free rectangular thin plates resting on elastic foundations by a new symplectic superposition method. Proc R Soc A. 2013;469(2153):20120681. doi:10.1098/rspa.2012.0681.

39. Li R, Wang H, Zheng X, Xiong S, Hu Z, Yan X, et al. New analytic buckling solutions of rectangular thin plates with two free adjacent edges by the symplectic superposition method. Eur J Mech A/Solids. 2019;76:247–62. doi:10.1016/j.euromechsol.2019.04.014.
40. Li R, Ni X, Cheng G. Symplectic superposition method for benchmark flexure solutions for rectangular thick plates. J Eng Mech. 2015;141(2):04014119. doi:10.1061/(asce)em.1943-7889.0000840.
41. Asemi K, Shariyat M. Three-dimensional biaxial post-buckling analysis of heterogeneous auxetic rectangular plates on elastic foundations by new criteria. Comput Meth Appl Mech Eng. 2016;302:1–26. doi:10.1016/j.cma.2015.12.026.
42. Asemi K, Shariyat M, Salehi M, Ashrafi H. A full compatible three-dimensional elasticity element for buckling analysis of FGM rectangular plates subjected to various combinations of biaxial normal and shear loads. Finite Elem Anal Des. 2013;74:9–21. doi:10.1016/j.finel.2013.05.011.
43. Kartam. Artificial neural networks for civil engineers. New York, NY, USA: American Society of Civil Engineers; 1997.
44. Adeli H. Neural networks in civil engineering: 1989–2000. Comput Aided Civ Infrastruct Eng. 2001;16(2):126–42. doi:10.1111/0885-9507.00219.
45. Salehi H, Burgueño R. Emerging artificial intelligence methods in structural engineering. Eng Struct. 2018;171:170–89. doi:10.1016/j.engstruct.2018.05.084.
46. Sun H, Burton HV, Huang H. Machine learning applications for building structural design and performance assessment: state-of-the-art review. J Build Eng. 2021;33(4):101816. doi:10.1016/j.jobe.2020.101816.
47. Thai HT. Machine learning for structural engineering: a state-of-the-art review. Structures. 2022;38:448–91. doi:10.1016/j.istruc.2022.02.003.
48. Hu D, Hu Y, Hu R, Tan Z, Ni P, Chen Y, et al. Machine learning-finite element mesh optimization-based modeling and prediction of excavation-induced shield tunnel ground settlement. Int J Comput Methods. 2025;22(4):2450066. doi:10.1142/s021987622450066x.
49. Zhu J, Wang X, Cao G, Xu L, Cao Y. Quantum interval neural network for uncertain structural static analysis. Int J Mech Sci. 2025;303:110646. doi:10.1016/j.ijmecsci.2025.110646.
50. Wang Z, Wang X. Quantum-classical hybrid genetic evolutionary algorithm for topology optimization of continuum structures. Int J Numer Meth Eng. 2025;126(13):e70073. doi:10.1002/nme.70073.
51. Xu Y, Wang X, Wang Z. Quantum mapping algorithm for structural non-probabilistic reliability optimization. Struct Multidiscip Optim. 2025;68(7):138. doi:10.1007/s00158-025-04085-w.
52. Xie WT, Song DN, Tang WC, Ma JW, Li JH. Auxiliary support path planning for robot-assisted machining of thin-walled parts with non-uniform thickness and closed cross-section based on a neutral surface. J Manuf Process. 2025;147:16–28. doi:10.1016/j.jmapro.2025.05.002.
53. Yang J, Liu Y, Lu X, Wang T. An adaptive measurement-based substructure identification framework for dynamic response reconstruction. Mech Syst Signal Process. 2025;239:113277. doi:10.1016/j.ymssp.2025.113277.
54. Cao Y, Chi H, Zhu Z, Fan S, Zhang Y, Tang Y, et al. Multi-functional self-sensing electronic gasket for structural health monitoring of transportation pipelines. Adv Funct Mater. 2025;35(20):2412634. doi:10.1002/adfm.202412634.
55. Ren K, Miao J, Qing H, Xu W, Zhang X, He Z, et al. Probing to dynamics of a tube-core sandwich enhanced liquid-filled tank subjected to hydrodynamic ram. Thin Walled Struct. 2025;215:113573. doi:10.1016/j.tws.2025.113573.
56. Guo K, Zhou S, Cai W, Mu M, Chen J, Zhu L. An analytical solution for dynamic plastic responses of PVC foam sandwich beams under ice impact. Thin Walled Struct. 2026;223:114647. doi:10.1016/j.tws.2026.114647.
57. Feng DC, Liu ZT, Wang XD, Chen Y, Chang JQ, Wei DF, et al. Machine learning-based compressive strength prediction for concrete: an adaptive boosting approach. Constr Build Mater. 2020;230(3):117000. doi:10.1016/j.conbuildmat.2019.117000.
58. Nguyen-Sy T, Wakim J, To QD, Vu MN, Nguyen TD, Nguyen TT. Predicting the compressive strength of concrete from its compositions and age using the extreme gradient boosting method. Constr Build Mater. 2020;260(5):119757. doi:10.1016/j.conbuildmat.2020.119757.

59. Kaloop MR, Kumar D, Samui P, Hu JW, Kim D. Compressive strength prediction of high-performance concrete using gradient tree boosting machine. Constr Build Mater. 2020;264(12):120198. doi:10.1016/j.conbuildmat.2020.120198.
60. Marani A, Nehdi ML. Machine learning prediction of compressive strength for phase change materials integrated cementitious composites. Constr Build Mater. 2020;265(7):120286. doi:10.1016/j.conbuildmat.2020.120286.
61. Mojtabaei SM, Becque J, Hajirasouliha I, Khandan R. Predicting the buckling behaviour of thin-walled structural elements using machine learning methods. Thin Walled Struct. 2023;184:110518. doi:10.1016/j.tws.2022.110518.
62. Duong HT, Phan HC, Tran TM, Dhar AS. Assessment of critical buckling load of functionally graded plates using artificial neural network modeling. Neural Comput Appl. 2021;33(23):16425–37. doi:10.1007/s00521-021-06238-6.
63. Degtyarev VV, Tsavdaridis KD. Buckling and ultimate load prediction models for perforated steel beams using machine learning algorithms. J Build Eng. 2022;51(2):104316. doi:10.1016/j.jobe.2022.104316.
64. Kaveh A, Dadras Eslamlou A, Javadi SM, Geran Malek N. Machine learning regression approaches for predicting the ultimate buckling load of variable-stiffness composite cylinders. Acta Mech. 2021;232(3):921–31. doi:10.1007/s00707-020-02878-2.
65. Ullah S, Zhang J, Bo H, Zhang J, Javed MF, Chen W. Buckling behavior of orthotropic thin plates using analytical and machine learning methods. Eng Struct. 2025;324:119376. doi:10.1016/j.engstruct.2024.119376.
66. Yang Y, Mu Z, Ge X. Machine learning-based prediction of elastic buckling coefficients on diagonally stiffened plate subjected to shear, bending, and compression. Sustainability. 2023;15(10):7815. doi:10.3390/su15107815.